




Original Article

# Direct Observation of Low Strain, High Rate Deformation of Cultured Brain Tissue During Primary Blast

EDWARD W. VOGEL III,<sup>1</sup> MATTHEW B. PANZER,<sup>2</sup> FATIMA N. MORALES,<sup>1</sup> NEVIN VARGHESE,<sup>1</sup>  
CAMERON R. BASS,<sup>3</sup> DAVID F. MEANEY,<sup>4</sup> and BARCLAY MORRISON III<sup>1</sup> 

<sup>1</sup>Department of Biomedical Engineering, Columbia University, 1210 Amsterdam Avenue, New York, NY 10027, USA; <sup>2</sup>Department of Mechanical and Aerospace Engineering, Center for Applied Biomechanics, University of Virginia, 4040 Lewis and Clark Dr., Charlottesville, VA 22911, USA; <sup>3</sup>Department of Biomedical Engineering, Duke University, 136 Hudson Hall, Durham, NC 27708, USA; and <sup>4</sup>Department of Bioengineering, University of Pennsylvania, 240 Skirkanich Hall, 210 S. 33rd St., Philadelphia, PA 19104-6392, USA

(Received 20 August 2019; accepted 8 December 2019)

Associate Editor Joel D. Stitzel oversaw the review of this article.

**Abstract**—The Veterans Health Administration determined that over 250,000 U.S. service members were diagnosed with a traumatic brain injury (TBI) between 2008 and 2018, of which a great proportion were due to blast exposure. Although the penetrating (secondary) and inertia-driven (tertiary) phases of blast-induced TBI (bTBI) have been studied thoroughly and are known to be injurious, primary blast brain injury has been less studied. We investigated the biomechanics of primary bTBI in our previously developed *in vitro* shock tube model with a fluid-filled sample receiver. Using stereoscopic, high-speed cameras and digital image correlation (DIC), we mapped the deformation of organotypic hippocampal slice cultures (OHSCs) following a range of blast exposures to characterize the induced strains. As blast exposure increased, tissue strain increased, although the levels remained relatively low (maximum < 9%), with strain rates between 25 and 85 s<sup>-1</sup>. Both strain magnitude and rate were highly correlated with the in-air blast impulse and in-fluid peak pressure parameters. Comparing biomechanical parameters to previously reported blast-induced electrophysiological dysfunction, a threshold for deficits in long-term potentiation (LTP) was observed for strains between 3.7 and 6.7% and strain rates between 25 and 33 s<sup>-1</sup>. This is the first study to experimentally determine primary blast-induced strain and strain rates in hippocampal tissue.

**Keywords**—Traumatic brain injury, *In vitro* studies, Military injury.

## INTRODUCTION

Blast-induced traumatic brain injury (bTBI) is a serious health concern for military personnel and civilians in areas of conflict around the world. Between 2008 and 2018, the Department of Defense determined that nearly 250,000 US service personnel were diagnosed with combat TBI, mainly mild TBI (mTBI) caused by blast.<sup>9</sup> The more frequent use of improvised explosive devices (IEDs) coupled with greater surveillance by medical professionals for brain injuries have increased the incidence of bTBI. The biomechanics of blast-induced TBI are complex and multi-phasic.<sup>3</sup> Primary blast injury is initiated by the interaction of the shock wave with the skull and the brain as the shock wave transits the head. Secondary blast injury is defined as both blunt and penetrating injury, caused by ejecta launched from the blast origin. Tertiary blast injury is driven by inertial forces loading the biological tissue through rapid acceleration/deceleration of the body due to blast. Although secondary and tertiary blast exposures are known to be injurious, the effect of primary blast in isolation is still debated.

Research into bTBI has increased over the last 20 years with studies using a variety of methods to model blast exposure. Previous bTBI studies using *in vivo* animal models have reported altered memory and cognition following injury.<sup>5,6,17–19,35,37</sup> Some of these studies assert that motion of the head, and hence inertial loading, was eliminated, thereby providing a model of pure primary blast loading, i.e., the shock wave only.<sup>5,6,17,19,35</sup> However, it is extremely difficult

Address correspondence to Barclay Morrison III, Department of Biomedical Engineering, Columbia University, 1210 Amsterdam Avenue, New York, NY 10027, USA. Electronic mail: bm2119@columbia.edu

to completely fix the head during blast exposure. Even when extra steps were taken to secure the head, significant head accelerations remained as revealed by analysis of high-speed video.<sup>5,17,18</sup> Therefore, it remains a considerable challenge to investigate pure primary blast in animal models. We expressly designed our *in vitro* injury model to eliminate inertia-driven acceleration, thus isolating primary blast exposure.<sup>10,30</sup> In a previous study using high-speed video analysis, we observed no bulk motion of the tissue within the receiver, confirming an absence of inertia-driven forces on the tissue sample.<sup>10</sup> However, hippocampal electrophysiological function (including long-term potentiation [LTP]), protein expression, and blood-brain barrier integrity were all negatively affected in this model.<sup>12,13,20,21,38,39</sup> We have undertaken this study in order to better understand the tissue biomechanics that drove the biological deficits.

Contemporary *in vitro* models of non-blast TBI injury cultures with deformations in the range of 20–50% strain applied at strain rates  $< 50 \text{ s}^{-1}$ .<sup>7,29</sup> Computational models of inertia-driven TBI have predicted deformations of similar strain magnitudes and rates.<sup>25</sup> Conversely, computational simulations of the head under shock wave loading have predicted that brain tissue deformation is  $\leq 10\%$ , but applied at higher rates from 12 to  $960 \text{ s}^{-1}$ .<sup>32,34</sup> Modeling of our *in vitro* receiver under shock tube loading predicted tissue strains of  $\leq 8\%$  at high-strain rates ( $80 \text{ s}^{-1}$ ); however, these biomechanics have not been confirmed experimentally.<sup>30</sup> The purpose of this study was to experimentally characterize the tissue biomechanics for correlation with electrophysiological function within organotypic hippocampal slice cultures (OHSCs) during shock wave loading in our *in vitro* blast injury model. We utilized a stereoscopic high-speed camera system, in combination with digital image correlation (DIC) to quantify strain histories for a range of shock exposures. We found that primary blast exposure induced low strains ( $< 9\%$ ) at high-strain rates ( $25\text{--}85 \text{ s}^{-1}$ ) in OHSCs *in vitro*, with peak tissue strain and rate occurring after the pressure wave had passed the sample in the fluid filled receiver. Blast-induced strains and rates were highly correlated with in-air blast impulse and in-fluid peak pressure parameters. We observed thresholds for electrophysiological dysfunction, defined by deficits in LTP, between 3.7–6.7% strain and  $25\text{--}33 \text{ s}^{-1}$  rate. This study experimentally confirmed computationally predicted strain magnitudes and rates using our *in vitro* blast model. Our findings provide biomechanical injury thresholds for future computational models of primary bTBI that will contribute to the design of protective equipment and diagnostic capabilities.

## MATERIALS AND METHODS

### *Organotypic Hippocampal Slice Culture*

All animal procedures were approved by the Columbia University Institutional Animal Care and Use Committee (IACUC). Organotypic hippocampal slice cultures were generated from P8-P10 Sprague Dawley rats as previously described.<sup>10,13,29,38</sup> In brief, the hippocampus was excised, cut into  $400 \mu\text{m}$  thick sections on a McIlwain tissue chopper (Ted Pella Inc., Redding, CA), and plated onto Millicell inserts (EMD Millipore, Billerica, MA) in Neurobasal medium supplemented with 2 mM GlutaMAX<sup>TM</sup>, 1X B27 supplement, 10 mM 4-(2-hydroxyethyl)-1-piperazineethanesulfonic acid (HEPES), and 25 mM D-glucose (Thermo Fisher, Waltham, MA). Cultures were fed every 2–3 days after plating with full serum medium, containing 50% Minimum Essential Medium, 25% Hank's Balanced Salt Solution, 25% heat inactivated horse serum, 2 mM GlutaMAX, 25 mM D-glucose, and 10 mM HEPES (Sigma-Aldrich). Cultures were maintained for 10–14 days prior to blast exposure.

### *Cell Death Measurement*

Propidium iodide (PI) fluorescence was used to assess tissue health prior to blast exposure, applying  $2.5 \mu\text{M}$  PI (Life Technologies) in serum-free medium to cultures immediately before blast exposure. Cell death was determined using MetaMorph (Molecular Devices, Downingtown, PA) according to published methods.<sup>7,10,13,38</sup> Cultures that exhibited greater than 5% cell death before blast-exposure were eliminated. Previous studies with this injury model have reported that blast injury at the levels used in this study caused minimal cell death.<sup>13,38</sup>

### *Primary Blast Exposure*

Blast injury methods have been described previously in detail.<sup>10,13,20,21,30,38,39</sup> For this study, we modified our previously described cylindrical fluid filled receiver with a transparent box; this transparent box was then also filled with water to minimize image distortion (during high-speed videography) caused by the fluid filled cylindrical column. Cultures were first lightly spray painted to create a stochastic fiducial pattern for strain analysis and then placed into sterile bags filled with serum-free medium that was pre-equilibrated with 5%  $\text{CO}_2$  at  $37^\circ\text{C}$ . Any air bubbles were fastidiously removed from the bag, which was sealed and placed into the receiver column. The receiver column was filled with pre-warmed water ( $37^\circ\text{C}$ ), sealed with a silicone membrane, and the shock tube was fired. Blast

exposure levels were chosen so that in-fluid peak pressure and duration parameters were minimally correlated ( $r^2 = 0.04$ ), to reduce the contribution of these variables to correlations of biomechanical parameters and biological deficits.<sup>10,13</sup> Piezoresistive pressure transducers (Endevco 8530B-500, San Juan Capistrano, CA, USA) recorded incident pressure at the shock tube exit. For the blast levels tested in this study (Levels 1–4), peak overpressure, duration, and impulse were recorded, processed, and quantified as previously described.<sup>10,13,21,38</sup> As a real world comparison, according to the Conventional Weapons Effect Program (ConWEP), the characteristics of our Level 1 blast is comparable to that of a M49A4 60-mm mortar round at a standoff distance of 0.25–2 m, and a Level 4 blast is comparable to that of a M117 bomb at a standoff distance of 10–15 m. For each blast level, a representative in-fluid pressure trace is presented in Fig. 1.

#### High-Speed Videography and Digital Image Correlation (DIC)

A pair of Fastcam SA-X2 charge-coupled device (CCD) cameras (Photron USA, San Diego, CA) captured stereophotogrammetric videos of OHSCs during blast exposure. A calibration cube (15 mm × 12 mm) established a global coordinate system to orient the cameras in 3D space. The two cameras simultaneously recorded the culture during blast exposure at 5000 frames per second (FPS) with a resolution of  $896 \times 896$  (20  $\mu\text{m}$  pixel size).

Digital image correlation (DIC) was used to map unique correlation areas, or sub-image, of the surface pattern on the hippocampal slices to identify the same location in the images from the left and right cameras (GOM, Brunswick, Germany). At each time step, the algorithm successively identified the location of the center of each sub-image in the left and right image. Knowing the global positions of the cameras relative to

the sample, the sub-image's location within both images was converted into a single set of 3D coordinates in real space. To calculate sub-image deformations, the 3D coordinates were transformed onto the surface of the culture using the assumption that the local neighborhood of a point can be well approximated by a tangential plane. The tangential plane was calculated separately for both the undeformed and deformed states, and then the points in the local neighborhood were projected perpendicularly onto the tangential plane. This transformation resulted in two sets of points on the tangential plane for the undeformed and deformed state.

Sub-image coordinates were tracked between the reference frame and the deformed frame; however, it was necessary to adjust the coordinate system between the reference and the deformed frame. The sub-image's deformed coordinate system was determined using a local neighborhood of measurement points around the sub-image center. At this point, the deformation gradient tensor ( $F$ ) can be constructed for each sub-image at each time step. Each deformation gradient was decomposed into the product of two tensors using the polar decomposition theorem (Eq. 1): a pure stretch tensor ( $U$ ) and a pure rotation matrix ( $R$ ).

$$F = R \cdot U \quad (1)$$

The stretch tensor was computed from the Cauchy–Strain tensor ( $C$ ) and the orthogonal rotation matrix (Eqs. 2–4).

$$C = F^T \cdot F = U^T \cdot R^T \cdot R \cdot U \quad (2)$$

$$R^T \cdot R = I \quad (3)$$

$$U = \sqrt{C} \quad (4)$$

The first eigenvalue of the stretch tensor yielded the maximum principal strain (MPS) within each sub-image

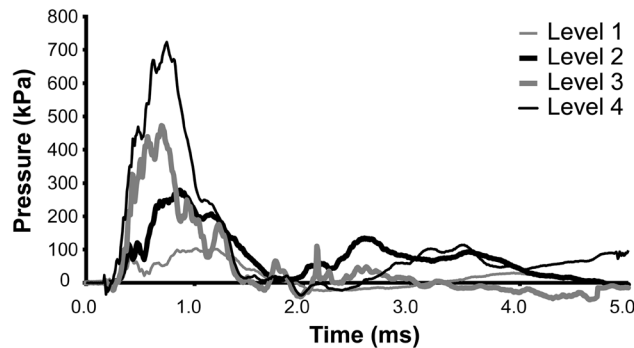


**FIGURE 1.** Representative in-fluid pressure profiles for blast exposures used in this study. The traces represent the in-fluid pressure profiles at the level of the sample for each of the blast levels tested in this study (Levels 1–4). Note that the duration of the pressure pulse is less than 5 ms.

plane at each time step. For all sub-images across the sample at each time, the MPS was averaged. Strain rate was calculated from the average MPS history. Both strain and strain rate across the range of blast intensities were analyzed by ANOVA, followed by Bonferroni *post hoc* tests with statistical significance set as  $p < 0.05$ . The Pearson correlation coefficient was calculated to determine with which blast parameters strain and rate were most highly correlated (duration, peak overpressure, and impulse measured in-air and in-fluid).

### Finite Element Simulation

We leveraged previously developed axisymmetric FE models of both the 1240 mm shock tube and the receiver to validate the mechanics of the system and the experienced tissue-level strains. The pressure time-histories at the exit of the shock tube and at the sample level were validated using the open-tube and in-receiver pressure time-histories from three levels of blast severity (Level 1, Level 3, and Level 4).<sup>13</sup> Following validation, the receiver FE model was used to investigate the strain response of a representative OHSC plated onto a Millicell insert.<sup>30</sup>

The mesh resolutions of both the shock tube and receiver were 1 mm, selected based on a previous mesh convergence study for shock tube modeling.<sup>31</sup> All element formulations and material constants were modeled after similar previously published finite element simulations of this shock tube, receiver, and OHSC. All FE analyses were performed using LS-DYNA hydrocode (v971.R5.1.1; Livermore Software Technologies Corp., Livermore, CA, USA). The accuracy of the modeled blast history to experimental data was assessed using the cross-correlation methods of correlation and analysis (CORA). For extracted strain data, mean individual integration points (IPT) MPS was calculated across three elements of the slice model and graphed for the first 5 ms of exposure.

## RESULTS

### Primary Blast Exposure Induced Low Strains

The initial rise in strain occurred over the first 2 ms of pressure loading; however, strain did not reach maximum magnitudes until the pressure pulse had transited the sample ( $> 3$  ms). After this point, strains were induced by deformation of the Millipore membrane as it vibrated like a drum head with limited bulk motion of the sample. We provided a time history of induced strains (Fig. 2) and footage of the first 30 ms following Level 4 blast exposure (Video 1) to visualize slice deformation during blast.

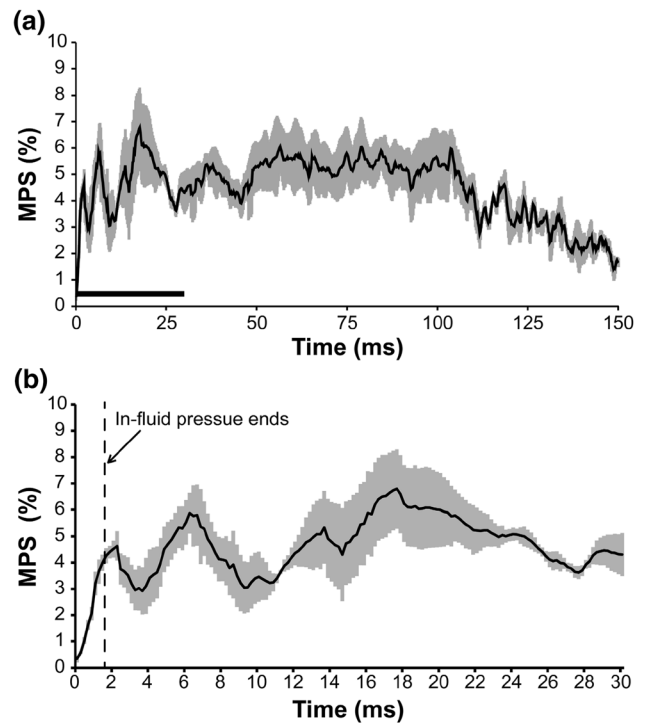


**FIGURE 2.** Time history of tissue strains induced by Level 4 blast exposure. (a) The trace represents the average maximum principal strain (MPS) on the tissue sample surface ( $\pm$  SEM,  $N = 3$ ) over the first 150 ms following Level 4 blast exposure. The black bar marks 30 ms after blast, which is expanded in (b). (b) The trace represents the MPS on the tissue sample surface ( $\pm$  SEM,  $N = 3$ ) over the first 30 ms following Level 4 blast exposure. The dotted vertical line indicates the time point when the in-fluid pressure transient passes the sample.

We observed that blast exposure induced strains of low magnitude ( $< 9\%$ ) (Fig. 3a). Level 1 blast exposure induced average maximum principal strains of  $3.7 \pm 0.4\%$ . Level 2 blast exposure significantly ( $p < 0.05$ ) increased strains to  $(6.7 \pm 0.6\%)$ , as compared to Level 1 blast. Level 3 ( $8.2 \pm 0.8\%$ ) and Level 4 ( $8.2 \pm 0.6\%$ ) blast exposures induced significantly ( $p < 0.05$ ) higher strains than Level 1 blast, but not Level 2 blast.

When compared to blast input parameters (Fig. 3b: duration, Fig. 3c: peak pressure, and Fig. 3d: impulse), strain best correlated with in-air impulse ( $R^2 = 0.91$ ) and in-fluid peak pressure ( $R^2 = 0.86$ ). Strain was somewhat correlated to in-fluid impulse ( $R^2 = 0.71$ ), but only weakly correlated to in-air pressure ( $R^2 = 0.44$ ), in-air duration ( $R^2 = 0.52$ ), and in-fluid duration ( $R^2 = 0.00$ ).

### Primary Blast Exposure Induced High-Strain Rates

Blast exposure above Level 2 significantly elevated maximum strain rate (Fig. 4a). Level 1 and Level 2 blast exposure induced average maximum strain rates

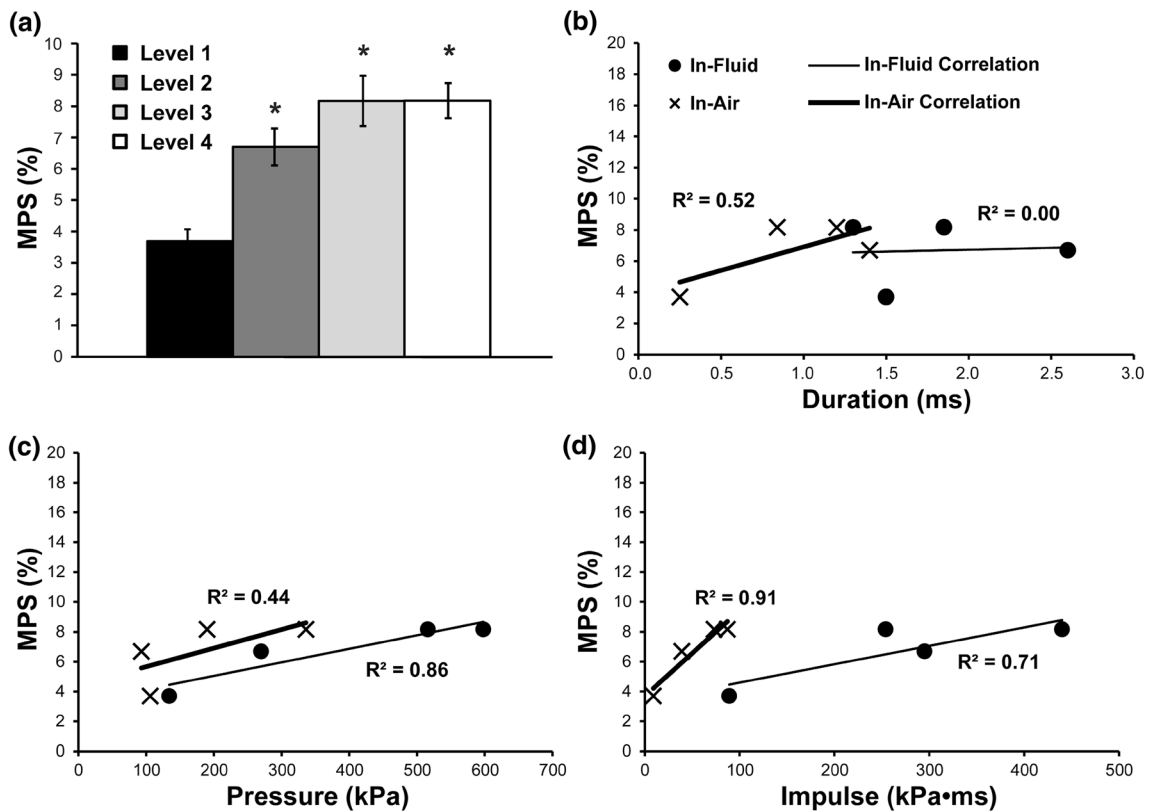


**FIGURE 3.** Primary blast exposure induced strains of low magnitudes. (a) Increasing blast exposure increased the average maximum principal strain (MPS) in OHSCs, but remained below 9% (mean  $\pm$  SEM;  $n = 3$ ,  $*p < 0.05$ , as compared to Level 1 blast). (b) Linear correlation between MPS and blast duration in-air and in-fluid, indicating a weak association with  $R^2 = 0.00$  and  $R^2 = 0.52$ , respectively. (c) Linear correlation between MPS and blast peak pressure, indicating a strong association with in-fluid ( $R^2 = 0.86$ ) and a weak association with in-air ( $R^2 = 0.44$ ) peak pressure. (d) Linear correlation between MPS and blast impulse indicating a strong association with in-air ( $R^2 = 0.91$ ) and a moderate association with in-fluid ( $R^2 = 0.71$ ) impulse.

of  $25.2 \pm 6.6$  and  $32.9 \pm 2.4 \text{ s}^{-1}$ , respectively. Level 3 blast exposure significantly increased strain rate ( $76.5 \pm 4.6 \text{ s}^{-1}$ ) as compared to Level 1 ( $p < 0.05$ ) and Level 2 ( $p < 0.05$ ) blast. Level 4 blast exposure induced significantly ( $p < 0.05$ ) higher strain rates ( $85.6 \pm 15.3 \text{ s}^{-1}$ ) than Level 1 ( $p < 0.05$ ) and Level 2 ( $p < 0.05$ ) blast.

When compared to blast input parameters (Fig. 4b: duration, Fig. 4c: peak pressure, and Fig. 4d: impulse), blast-induced strain rates best correlated with in-fluid pressure ( $R^2 = 0.97$ ) and in-air impulse ( $R^2 = 0.93$ ). Strain rate was somewhat correlated to in-air pressure ( $R^2 = 0.80$ ) but only weakly correlated with in-fluid impulse ( $R^2 = 0.54$ ), in-air duration ( $R^2 = 0.08$ ), and in-fluid duration ( $R^2 = 0.12$ ).

#### Strain and Rate Thresholds for Blast-Induced LTP Deficits

We then compared the measured strain and strain rates at these blast levels to potentiation at the same blast intensities measured previously.<sup>38</sup> After a Level 1 blast (applied strain of 3.7% at  $25.2 \text{ s}^{-1}$ ), LTP

( $46.9 \pm 10.5\%$ ) was not different from sham cultures (Fig. 5); however, after a Level 2 blast (applied strain of 6.7% at  $32.9 \text{ s}^{-1}$ ), LTP ( $17.6 \pm 8.8\%$ ) was significantly reduced. As the blast severity increased, LTP was further reduced. After a Level 3 blast (applied strain of 8.2% at  $76.5 \text{ s}^{-1}$ ), LTP ( $12.6 \pm 3.1\%$ ) was significantly reduced. After a Level 4 blast (applied strain of 8.2% at  $85.6 \text{ s}^{-1}$ ), LTP ( $3.4 \pm 13.1\%$ ) was significantly reduced. Potentiation was strongly and negatively correlated with strain ( $R^2 = 0.88$ ) and was moderately and negatively correlated with strain rate ( $R^2 = 0.81$ ).

Additionally, we compared the measured in-air and in-fluid pressures, durations, and impulses at these blast levels to potentiation at the same blast intensities measured previously.<sup>38</sup> Potentiation was strongly and negatively correlated with both in-air ( $R^2 = 0.93$ ) and in-fluid impulse ( $R^2 = 0.93$ ). Potentiation was moderately and negatively correlated with both in-air ( $R^2 = 0.68$ ) and in-fluid peak pressure ( $R^2 = 0.89$ ) and in-air duration ( $R^2 = 0.69$ ). Potentiation was weakly and negatively correlated with in-fluid duration ( $R^2 = 0.41$ ).

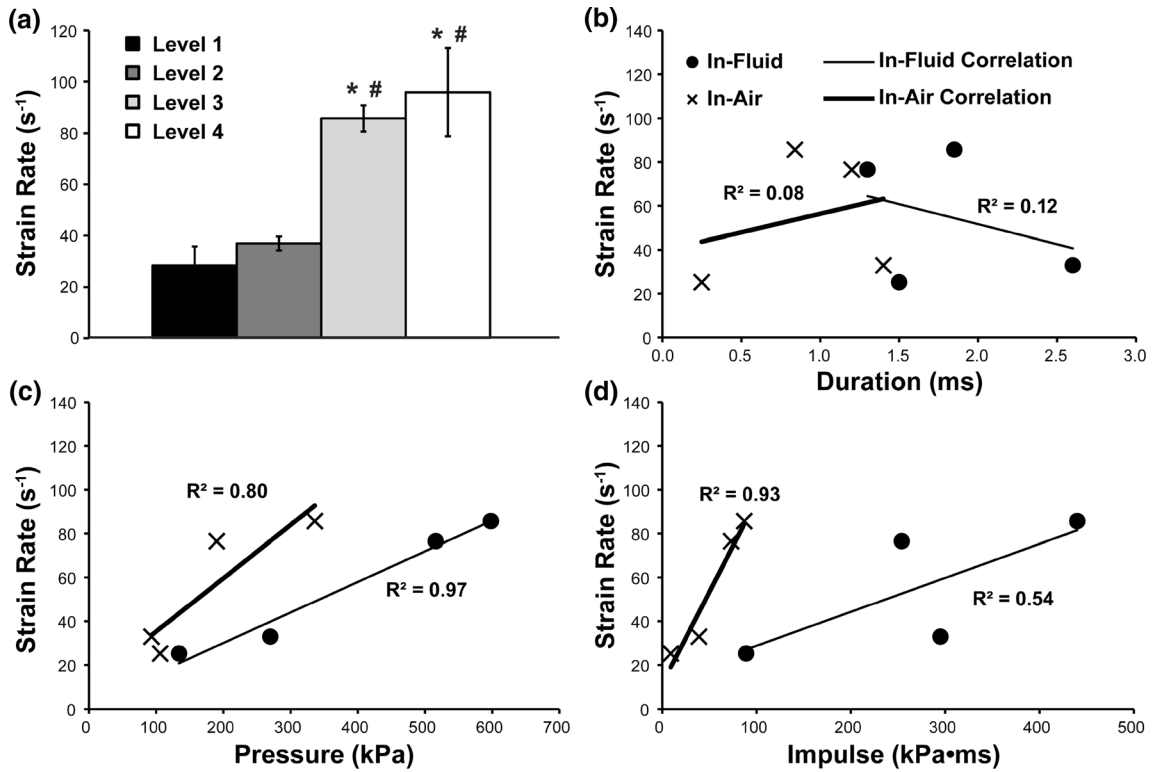


**FIGURE 4.** Primary blast exposure induced deformations with strain rates in excess of  $80 \text{ s}^{-1}$ . (a) Increasing blast exposure increased the average peak strain rate in OHSCs. Both Level 3 and Level 4 blast exposures induced significantly greater strain rates over both Level 1 and Level 2 blast. (mean  $\pm$  SEM;  $n = 3$ ,  $*p < 0.05$ , as compared to Level 1 blast,  $\#p < 0.05$  as compared to Level 2 blast). (b) Linear correlation between strain rate and blast duration in-air and in-fluid, indicating a weak association with  $R^2 = 0.08$  and  $R^2 = 0.12$ , respectively. (c) Linear correlation between strain rate and blast peak pressure indicating a strong association with in-fluid ( $R^2 = 0.97$ ) and a moderate association with in-air ( $R^2 = 0.80$ ) pressure. (d) Linear correlation between strain rate and blast impulse indicating a strong association with in-air ( $R^2 = 0.93$ ) and a weak association with in-fluid ( $R^2 = 0.54$ ) impulse.

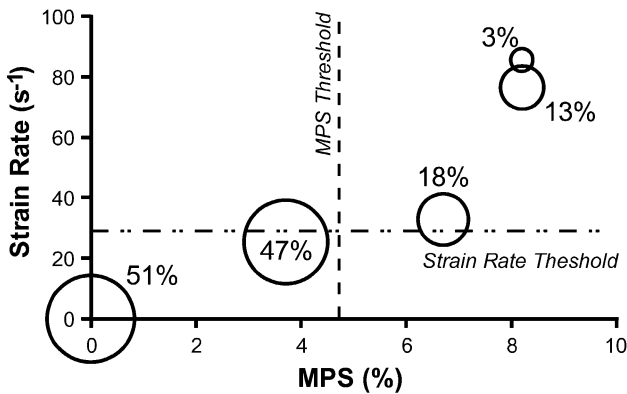


**FIGURE 5.** Increased strain magnitude and rate reduced long-term potentiation (LTP). We observed a threshold for significant LTP deficits between 3.7 and 6.7% MPS. We observed a threshold for LTP deficits for strain rates between 25 and  $33 \text{ s}^{-1}$ .

*Finite Element Modeling Matched Observed Pressure Time-Histories and Induced Strains*

The shock tube FE model produced responses that were strong predictions of the experimental results,

and nearly 90% of the model pressure time-history data for all blast levels simulated fit within the experimental corridors (data not shown). The in-air pressure time-histories over the first 5 ms of exposure for Level 1, Level 3, and Level 4 blast were corroborated with CORA scores of 0.87, 0.90, and 0.90, respectively.

The receiver FE model also predicted the experimental response of the receiver capturing similar pressure dynamics as previous tests with same modeled experimental setup.<sup>30</sup> The modeled pressure wave was also an excellent fit with the experimental data, validating the fluid-structure interaction between the shock tube model and the receiver model. The in-fluid pressure time-histories over the first 5 ms of exposure for Level 1 (Fig. 6a), Level 3 (Fig. 6b) and Level 4 (Fig. 6c) blast were corroborated with CORA scores of 0.69, 0.86, and 0.83, respectively. Although the modeled pressure time-histories over the first 5 ms of exposure correlated strongly with experimental results, the maximum average strain (Fig. 6d) in the modeled OHSC remained lower than experimental results for all three tested blast exposures (Level 1: 0.7%, Level 3:

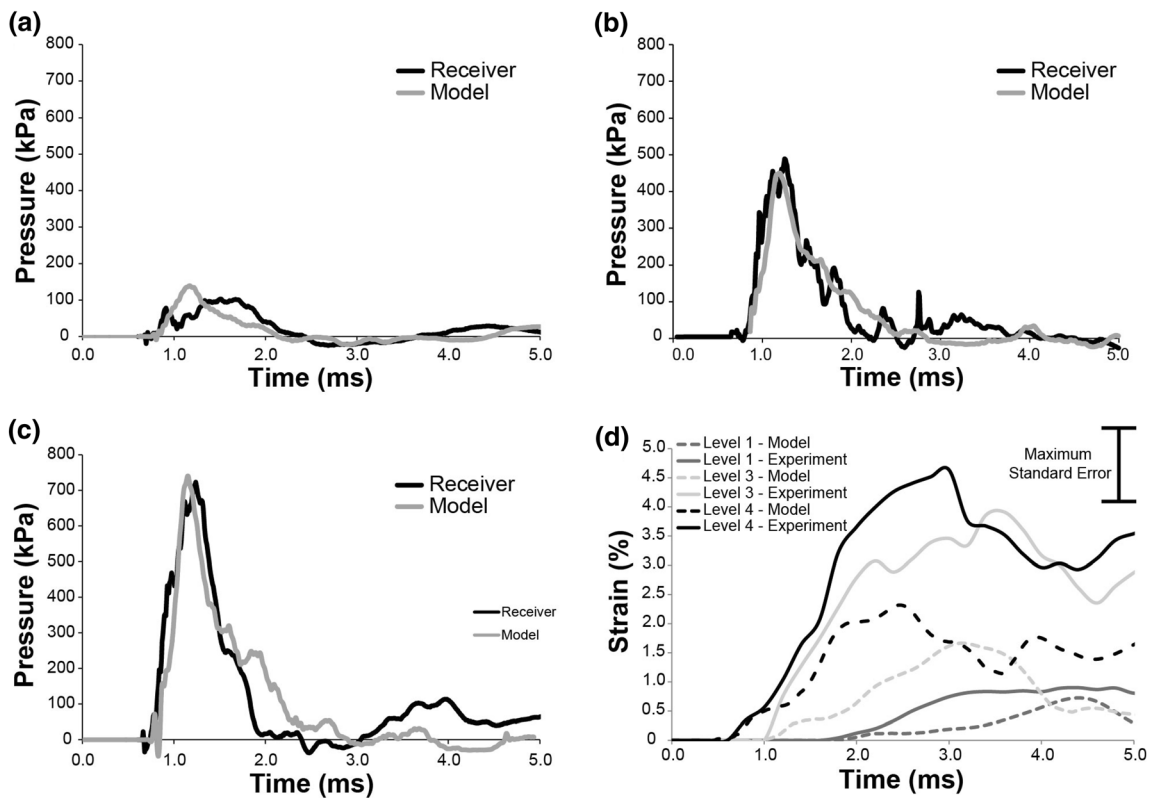


**FIGURE 6.** Comparison of experimental data with simulation results. The modeled pressure wave was an excellent fit to the experimental data, validating the fluid–structure interaction between the shock tube model and the receiver model. The in-fluid pressure time-histories over the first 5 ms of exposure for (a) Level 1, (b) Level 3, and (c) Level 4 are presented; the CORA score for the Level 1, Level 3, and Level 4 simulations were 0.69, 0.86, and 0.83, respectively, indicating excellent agreement. (d) The predicted strain histories in an OHSC over the first 5 ms of exposure are presented with experimentally measured strains. Predicted maximum average strains were 0.7, 1.7, and 2.3% with experimentally measured maximum average strains of 0.9, 3.9, and 4.6% for Level 1, Level 3, and Level 4, respectively. Error bars are not included here for the sake of clarity, and maximum standard error is shown instead.

1.7%, Level 4: 2.3%); however, there was a similar, large increase in modeled strain from Level 1 to Level 3 (Level 3: 142% higher than Level 1) and a similar, modest increase from Level 3 to Level 4 (Level 4: 35% higher than Level 3), as also measured in the experimental measurements.

## DISCUSSION

This is the first study to experimentally measure primary blast-induced strain and strain rates in hippocampal tissue. We observed a strain threshold for LTP deficits between 3.7 and 6.7% and a strain rate threshold between 25 and 33 s<sup>-1</sup>. The observed tissue strain and rate were well predicted computationally for this injury model by Panzer and colleagues (< 8%, ~ 80 s<sup>-1</sup>), similarly observing maximum strains after the pressure wave had passed the sample. Our experimental validation improves our understanding of tolerance criteria for neurological deficits in response to primary blast exposure. Ultimately, an

understanding of these tolerance criteria can lead to the development of improved armor and helmets for military personnel in theater.

Although no other study has experimentally quantified strain fields in brain tissue following blast exposure, one study found that shock loading of a poly-(methyl methacrylate)/Perma-Gel model of a human skull/brain induced 4.5% strain or less within the Perma-Gel.<sup>1</sup> Although strain rates were not explicitly reported, the study reported that loading occurred at high-strain rates. Peak pressures in the gel were 350 kPa, which is slightly greater than our Level 2 blast that induced 6% strain. Another study employed a split-Hopkinson bar to induce strain rates of over 8000 s<sup>-1</sup>, across a range of strains (3–42%), in acute coronal brain slices embedded in gelatin blocks.<sup>33</sup> Although the pressure transient at the tissue level exhibited a similar rise-time (~ 300 μs) and duration (~ 1 ms) applied in our study, the peak pressures within the aCSF greatly exceeded those within the receiver from our study (11 MPa vs. 0.6 MPa). Average

maximum principal strains in that study were 28%, which subsequently damaged neurons in CA1 when observed 6 h post-injury. Although that study corroborates our finding that increased fluid pressures caused elevated strains and strain rates, the strain and rates greatly exceeded those in our study, which could explain the differences in observed cell death between the models.<sup>13</sup>

Multiple studies have computationally modeled blast exposure for both *in vitro* and *in vivo* loading scenarios.<sup>3,25,30,32</sup> The experimental blast pressure time-histories utilized in this study were compared to finite element modeling. Modeled average strain levels in the tissue were aligned with experimental data (Fig. 6d) in that they remained low ( $< 3\%$ ); however, it is important to note that modeled strains were all lower than strains measured experimentally ( $< 5\%$ ). Panzer and colleagues predicted that shock loading of tissues in our *in vitro* receiver would induce MPS less than 8% and maximum strain rates of  $80 \text{ s}^{-1}$  or less, which aligns closely with our findings.<sup>30</sup> Computational models of the human head under shock loading corroborated the biomechanical loading observed with our injury model.<sup>15,32,34</sup> Those studies predicted maximum strains below 10% and maximum strain rates to reach between 10 and  $570 \text{ s}^{-1}$ , depending on loading conditions. The same study predicted that strain was mainly dependent on the impulse of the blast, which was corroborated with our experimental findings (Fig. 3d).<sup>32</sup> We have previously reported that biological outcomes such as LTP and blood-brain barrier disruption were also dependent on the impulse of the blast wave.<sup>13,21</sup> In the aforementioned computational studies, maximum strains were observed after the pressure pulse had passed through the *in vitro* sample or the skull/brain model. Although our study corroborated this result, video analysis suggested that blast-induced deformation was driven by vibration of the Millipore membrane, on which the culture was adhered, within the test apparatus. This result may have been driven by bulk fluid motion within the column, which was observed in computational models of the receiver, as well.<sup>30</sup>

Comparing the strain field induced by primary blast vs. tertiary blast, *in vitro* and *in vivo* studies have reported that inertial-driven TBI leads to higher strain magnitudes, but lower strain rates than what we report for primary blast. One common methodology for mimicking inertial-driven strains is stretching of cultured cells or tissue by deformation of the culture substrate. In these studies, applied strains range from 1 to 140% whereas strain rates remained below  $50 \text{ s}^{-1}$ .<sup>16,27,29</sup> Alternatively, shearing devices have been developed for 3D cell cultures, capable of inducing up to 50% shear strain at rates from 1 to  $30 \text{ s}^{-1}$ .<sup>26</sup> An-

other study utilized magnetic resonance imaging (MRI) to quantify the strain field applied using an *in vivo* brain impact device.<sup>4</sup> In this study, MPS ranged from 20 to 40% in certain regions, applied at rates between 10 and  $40 \text{ s}^{-1}$ . Most computational simulations predicted that impact or accelerative forces on human head models induced high-strain magnitudes (6–96%) and low strain rates ( $< 80 \text{ s}^{-1}$ ).<sup>8,36</sup> Interestingly, computational models of controlled cortical impact (CCI), a commonly used blunt-impact injury model, predicted high-strain magnitudes (5–60%) and strain rates ( $> 400 \text{ s}^{-1}$ ).<sup>8,28</sup> Since the strain rate differs greatly from other experimental and computational models of inertial TBI, injury biomechanics should be considered when comparing CCI-induced pathobiology to other TBI models and when interpreting pathobiological or behavioral outcomes following exposure to brain injury, like primary blast.

In this study, we correlated our previously reported levels of LTP following *in vitro* blast to the induced strain magnitudes and strain rates at the same levels.<sup>38</sup> From the correlations, blast-induced LTP deficits were dependent on both strain and strain rate, with strains above 3.7% and strain rates above  $25 \text{ s}^{-1}$  inducing significant LTP deficits. Although no other study has investigated LTP deficits at high-strain rates, our group has previously observed that a single mild stretch injury (12%,  $5\text{--}6 \text{ s}^{-1}$ ) did not affect LTP; however, a subsequent mild stretch delivered 24 h after the first significantly reduced LTP without altering other evoked response measures.<sup>11</sup> It is possible that the observed strain threshold for LTP deficits in our study, the result of bulk fluid motion causing mechanical deformations of the Millipore membrane substrate, is lower since the primary blast injury model deforms tissue at higher rates than the stretch injury model. In other words, the overarching contribution to the observed LTP deficits may be due to the higher strain rate induced by blast injury. Although LTP was not investigated, another stretch injury study found that the strain threshold for electrophysiological dysfunction was potentially as low as 5% when stretched at  $5 \text{ s}^{-1}$ .<sup>41</sup> Upon mathematically fitting functional changes to applied strain/rate injury parameters, Kang and colleagues found that most changes to basal hippocampal and cortical electrophysiological dysfunction were dependent on both strain magnitude and rate, even at low strain magnitudes.<sup>22,23</sup> Another study observed that changing the rate of stretching hippocampal cultures, increasing from 1 to 5 to  $50 \text{ s}^{-1}$ , while maintaining low strain magnitudes ( $< 6\%$ ) increased cytosolic  $[\text{Ca}^{2+}]$ , an important parameter for LTP induction.<sup>27</sup> Previous studies hypothesized that macro- and micro-interfaces between cellular structures with disparate properties, e.g., the dendritic



spines and transmembrane structures critical to LTP induction, could be particularly vulnerable to damage from high-strain rate loading.<sup>14,26</sup>

It has been shown that electrophysiological dysfunction can occur even in the absence of cell death; however, multiple experimental studies have similarly investigated strain thresholds for cell death.<sup>2,7,13,28</sup> Biomechanical thresholds for electrophysiological dysfunction and cellular death are critical to the advancement of computational TBI models. Current finite element models of the human head can incorporate a neural tract structure, identified by diffusion tensor imaging, to predict the effect of injury on neural connections.<sup>24,40</sup> For example, Kraft and colleagues found that 20% of the neural connectome links between brain regions were fully degraded by 96 h after a frontal TBI, when using an axonal strain threshold (18%) for functional deficits identified *in vitro*.<sup>2,24</sup> Our study connects blast parameters (peak pressure, duration, impulse) to biomechanical deformation (strain magnitude, rate) and provides computational studies with additional threshold information to better inform their models.

Although our study provided insights into the biomechanics of primary blast injury, there are several limitations that should be considered. The DIC software required that a fiducial pattern be applied to the OHSCs so that sub-images can be assigned for subsequent deformation tracking. It is possible that the spray paint used to make that pattern altered the physical properties of the OHSC and, thus, the strain response. Additionally, the use of spray paint prevented subsequent electrophysiological recording and imaging of the patterned slices. In the future, different biological dyes or staining could be implemented to determine whether the induced strains were altered by the paint and to determine electrophysiological activity and image slices after blast injury. For the construction of the fluid-filled receiver, a square box was built to surround the receiver and filled with water, to prevent image distortion that accompanies recording a sample through a cylindrical PVC receiver. This structure served to better match the refractive indices of the intervening media, PVC ( $n = 1.5390$ ) and water ( $n = 1.33$ ) and present a flat surface through which to image, minimizing image-distortion and allowing for proper calibration of the system. A more ideal setup would be to redesign the fluid-filled receiver with a square column. An inherent limitation of any stereophotogrammetric technique is that only strains on visible surfaces were measured, although, this may not be a significant limitation because the OHSCs are a few hundred microns thick. Recording speed was limited by lighting conditions, which were somewhat limited by space constraints around the receiver. The onset time of the in-fluid pressure transient at the level

of the sample was approximately 500  $\mu\text{s}$ , which allows capture of this onset in only two frames. Although the maximum strain magnitudes and rates were observed after pressure loading had subsided, a higher frame rate would be desirable in future studies.

In summary, we report that *in vitro* primary blast exposure induced low strain magnitudes and high-strain rates in OHSCs with strain magnitudes between 3–9% and rates between 25–86  $\text{s}^{-1}$  for Level 1–4 blasts. Both strain magnitude and rate were highly correlated with in-air blast impulse and in-fluid peak pressure. Peak tissue strains and rates were observed after the pressure wave had passed the sample, suggesting that this mode of strain was driven by either bulk fluid motion or vibration of the culture substrate like a drum head. Our results aligned closely with computational simulations of our blast injury device under shock loading.<sup>30</sup> When comparing biomechanical parameters to blast-induced LTP deficits, we observed that a strain magnitude and rate threshold for LTP-loss was found between 3.7–6.7% and 25–33  $\text{s}^{-1}$ , respectively. The reported findings will advance computational modeling of the brain under shock loading by providing tissue-level tolerance criteria for neuronal dysfunction.

## ELECTRONIC SUPPLEMENTARY MATERIAL

The online version of this article (<https://doi.org/10.1007/s10439-019-02437-4>) contains supplementary material, which is available to authorized users.

## ACKNOWLEDGMENTS

This work was supported in part by a Multidisciplinary University Research Initiative from the Army Research Office (W911NF-10-1-0526), a Defense University Research Instrumentation Program (DURIP) grant from the Office of Naval Research (N00014-14-1-0750), and by a National Defense Science & Engineering Graduate Fellowship from the Department of Defense (EWV-2012).

## DISCLOSURES

The authors declare no competing financial interests.

## REFERENCES

- Alley, M. D., B. R. Schimizza, and S. F. Son. Experimental modeling of explosive blast-related traumatic brain injuries. *Neuroimage* 54(Suppl 1):S45–S54, 2011.

- <sup>2</sup>Bain, A. C., and D. F. Meaney. Tissue-level thresholds for axonal damage in an experimental model of central nervous system white matter injury. *J. Biomech. Eng.* 122:615–622, 2000.
- <sup>3</sup>Bass, C. R., M. B. Panzer, K. A. Rafaels, G. Wood, J. Shridharani, and B. P. Capeheart. Brain injuries from blast. *Ann. Biomed. Eng.* 40:185–202, 2012.
- <sup>4</sup>Bayly, P. V., E. B. Black, R. C. Pedersen, E. P. Leister, and G. M. Genin. In vivo imaging of rapid deformation and strain in an animal model of traumatic brain injury. *J. Biomech.* 39:1086–1095, 2006.
- <sup>5</sup>Beamer, M., S. R. Tummala, D. Gullotti, K. Kopil, S. Gorka, T. Abel, C. R. Bass, B. Morrison, III, A. S. Cohen, and D. F. Meaney. Primary blast injury causes cognitive impairments and hippocampal circuit alterations. *Exp. Neurol.* 283:16–28, 2016.
- <sup>6</sup>Budde, M. D., A. Shah, M. McCrea, W. E. Cullinan, F. A. Pintar, and B. D. Stemper. Primary blast traumatic brain injury in the rat: relating diffusion tensor imaging and behavior. *Front. Neurol.* 4:1–12, 2013.
- <sup>7</sup>Cater, H. L., L. E. Sundstrom, and B. Morrison, III. Temporal development of hippocampal cell death is dependent on tissue strain but not strain rate. *J. Biomech.* 39:2810–2818, 2006.
- <sup>8</sup>Chen, Y. C., H. Mao, K. H. Yang, T. Abel, and D. F. Meaney. A modified controlled cortical impact technique to model mild traumatic brain injury mechanics in mice. *Front. Neurol.* 5:1–14, 2014.
- <sup>9</sup>DVBIC. Department of Defense Numbers for Traumatic Brain Injury. Defense and Veterans Brain Injury Center (DVBIC). Silver Spring: Armed Forces Health Surveillance Center, 2018.
- <sup>10</sup>Effgen, G. B., C. D. Hue, E. W. Vogel, III, M. B. Panzer, C. R. Bass, D. F. Meaney, and B. Morrison, III. A multiscale approach to blast neurotrauma modeling: part II: methodology for inducing blast injury to in vitro models. *Front. Neurol.* 3:1–10, 2012.
- <sup>11</sup>Effgen, G. B., and B. Morrison, III. Electrophysiological and pathological characterization of the period of heightened vulnerability to repetitive injury in an *in vitro* stretch model. *J. Neurotrauma* 34:914–924, 2016.
- <sup>12</sup>Effgen, G. B., T. Ong, S. Nammalwar, A. I. Ortuno, D. F. Meaney, C. R. Bass, and B. Morrison, III. Primary blast exposure increases hippocampal vulnerability to subsequent exposure: reducing long-term potentiation. *J. Neurotrauma* 33:1901–1912, 2016.
- <sup>13</sup>Effgen, G. B., E. W. Vogel, III, K. A. Lynch, A. Lobel, C. D. Hue, D. F. Meaney, C. R. Bass, and B. Morrison, III. Isolated primary blast alters neuronal function with minimal cell death in organotypic hippocampal slice cultures. *J. Neurotrauma* 31:1202–1210, 2014.
- <sup>14</sup>Elkin, B. S., E. U. Azeloglu, K. D. Costa, and B. Morrison, III. Mechanical heterogeneity of the rat hippocampus measured by AFM indentation. *J. Neurotrauma* 24:812–822, 2007.
- <sup>15</sup>Garimella, H. T., R. H. Kraft, and A. J. Przekwas. Do blast induced skull flexures result in axonal deformation? *PLoS ONE* 13:e0190881, 2018.
- <sup>16</sup>Geddes, D. M., R. S. Cargill, and M. C. LaPlaca. Mechanical stretch to neurons results in a strain rate and magnitude-dependent increase in plasma membrane permeability. *J. Neurotrauma* 20:1039–1049, 2003.
- <sup>17</sup>Goldstein, L. E., A. M. Fisher, C. A. Tagge, X. L. Zhang, L. Velisek, J. A. Sullivan, C. Upreti, J. M. Kracht, M. Ericsson, M. W. Wojnarowicz, C. J. Goletiani, G. M. Maglakelidze, N. Casey, J. A. Moncaster, O. Minaeva, R. D. Moir, C. J. Nowinski, R. A. Stern, R. C. Cantu, J. Geiling, J. K. Blusztajn, B. L. Wolozin, T. Ikezu, T. D. Stein, A. E. Budson, N. W. Kowall, D. Chargin, A. Sharon, S. Saman, G. F. Hall, W. C. Moss, R. O. Cleveland, R. E. Tanzi, P. K. Stanton, and A. C. McKee. Chronic traumatic encephalopathy in blast-exposed military veterans and a blast neurotrauma mouse model. *Sci. Transl. Med.* 4:134–160, 2012.
- <sup>18</sup>Gullotti, D. M., M. Beamer, M. B. Panzer, Y. Chia Chen, T. P. Patel, A. Yu, N. Jaumard, B. Winkelstein, C. R. Bass, B. Morrison, and D. F. Meaney. Significant head accelerations can influence immediate neurological impairments in a murine model of blast-induced traumatic brain injury. *J. Biomech. Eng.* 136:91004, 2014.
- <sup>19</sup>Heldt, S. A., A. J. Elberger, Y. Deng, N. H. Guley, N. Del Mar, J. Rogers, G. C. Choi, J. Ferrell, T. S. Rex, M. G. Honig, and A. Reiner. A novel closed-head model of mild traumatic brain injury caused by primary overpressure blast to the cranium produces sustained emotional deficits in mice. *Front. Neurol.* 5:1–14, 2014.
- <sup>20</sup>Hue, C. D., S. Cao, C. R. Bass, D. F. Meaney, and B. Morrison, III. Repeated primary blast injury causes delayed recovery, but not additive disruption, in an *in vitro* blood-brain barrier model. *J. Neurotrauma* 31:951–960, 2014.
- <sup>21</sup>Hue, C. D., S. Cao, S. F. Haider, K. V. Vo, G. B. Effgen, E. W. Vogel, III, M. B. Panzer, C. R. Bass, D. F. Meaney, and B. Morrison, III. Blood-brain barrier dysfunction after primary blast injury *in vitro*. *J. Neurotrauma* 30:1652–1663, 2013.
- <sup>22</sup>Kang, W. H., and B. Morrison, III. Functional tolerance to mechanical deformation developed from organotypic hippocampal slice cultures. *Biomech. Model. Mechanobiol.* 14(3):561–575, 2014.
- <sup>23</sup>Kang, W. H., and B. Morrison, III. Predicting changes in cortical electrophysiological function after *in vitro* traumatic brain injury. *Biomech. Model. Mechanobiol.* 14(5):1033–1044, 2015.
- <sup>24</sup>Kraft, R. H., P. J. Mckee, A. M. Dagro, and S. T. Grafton. Combining the finite element method with structural connectome-based analysis for modeling neurotrauma: connectome neurotrauma mechanics. *PLoS Comput. Biol.* 8:1–15, 2012.
- <sup>25</sup>Lamy, M., D. Baumgartner, N. Yoganandan, B. D. Stemper, and R. Willinger. Experimentally validated three-dimensional finite element model of the rat for mild traumatic brain injury. *Med. Biol. Eng. Comput.* 51:353–365, 2013.
- <sup>26</sup>LaPlaca, M. C., D. K. Cullen, J. J. McLoughlin, and R. S. Cargill. High rate shear strain of three-dimensional neural cell cultures: a new *in vitro* traumatic brain injury model. *J. Biomech.* 38:1093–1105, 2005.
- <sup>27</sup>Lusardi, T. A., J. A. Wolf, M. E. Putt, D. H. Smith, and D. F. Meaney. Effect of acute calcium influx after mechanical stretch injury *in vitro* on the viability of hippocampal neurons. *J. Neurotrauma* 21:61–72, 2004.
- <sup>28</sup>Mao, H., L. Zhang, K. H. Yang, and A. I. King. Application of a finite element model of the brain to study traumatic brain injury mechanisms in the rat. *Stapp Car Crash J.* 50:583–600, 2006.
- <sup>29</sup>Morrison, III, B., H. L. Cater, C. D. Benham, and L. E. Sundstrom. An *in vitro* model of traumatic brain injury utilizing two-dimensional stretch of organotypic hippocampal slice cultures. *J. Neurosci. Methods* 150:192–201, 2006.

- <sup>30</sup>Panzer, M. B., K. A. Matthews, A. W. Yu, B. Morrison, III, D. F. Meaney, and C. R. Bass. A multiscale approach to blast neurotrauma modeling: Part I—development of novel test devices for in vivo and in vitro blast injury models. *Front. Neurol.* 3:46, 2012.
- <sup>31</sup>Panzer, M. B., B. S. Myers, and C. R. Bass. Mesh considerations for finite element blast modeling in biomechanics. *Comput. Methods Biomech. Biomed. Eng.* 16:612–621, 2013.
- <sup>32</sup>Panzer, M. B., B. S. Myers, B. P. Capehart, and C. R. Bass. Development of a finite element model for blast brain injury and the effects of CSF cavitation. *Ann. Biomed. Eng.* 40:1530–1544, 2012.
- <sup>33</sup>Sarnitoranont, M., S. J. Lee, Y. Hong, M. A. King, G. Subhash, J. Kwon, and D. F. Moore. High-strain-rate brain injury model using submerged acute rat brain tissue slice. *J. Neurotrauma* 29:418–429, 2012.
- <sup>34</sup>Singh, D., D. S. Cronin, and T. N. Haladuick. Head and brain response to blast using sagittal and transverse finite element models. *Int. J. Numer. Methods Biomed. Eng.* 30:470–489, 2014.
- <sup>35</sup>Stemper, B. D., A. S. Shah, M. D. Budde, C. M. Olsen, A. Glavaski-Josimovic, S. N. Kurpad, M. McCrea, and F. A. Pintar. Behavioral outcomes differ between rotational acceleration and blast mechanisms of mild traumatic brain injury. *Front. Neurol.* 7:1–13, 2016.
- <sup>36</sup>Takhounts, E., S. A. Ridella, V. Hasija, R. E. Tannous, J. Q. Campbell, D. Malone, K. Danelson, J. Stitzel, S. Rowson, and S. Duma. Investigation of traumatic brain injuries using the next generation of simulated injury monitor (SIMon) finite element head model. *Stapp Car Crash J.* 52:1–31, 2008.
- <sup>37</sup>Vandevord, P. J., R. Bolander, V. S. S. S. Sajja, K. Hay, and C. A. Bir. Mild neurotrauma indicates a range-specific pressure response to low level shock wave exposure. *Ann. Biomed. Eng.* 40:227–236, 2012.
- <sup>38</sup>Vogel, III, E. W., G. B. Effgen, T. P. Patel, D. F. Meaney, C. R. Bass, and B. Morrison, III. Isolated primary blast inhibits long-term potentiation in organotypic hippocampal slice cultures. *J. Neurotrauma* 33:652–661, 2016.
- <sup>39</sup>Vogel, III, E. W., S. H. Rwema, D. F. Meaney, C. R. Bass, and B. Morrison, III. Primary blast injury depressed hippocampal long-term potentiation through disruption of synaptic proteins. *J. Neurotrauma* 34(5):1063–1073, 2016.
- <sup>40</sup>Wright, R. M., A. Post, B. Hoshizaki, and K. T. Ramesh. A multiscale computational approach to estimating axonal damage under inertial loading of the head. *J. Neurotrauma* 30:102–118, 2013.
- <sup>41</sup>Yu, Z., and B. Morrison, III. Experimental mild traumatic brain injury induces functional alteration of the developing hippocampus. *J. Neurophysiol.* 103:499–510, 2010.

**Publisher's Note** Springer Nature remains neutral with regard to jurisdictional claims in published maps and institutional affiliations.